

Hyperfine constants of low-lying states of $^{135}\text{Ba}^+$

Kai-zhi Yu

School of Physics and Telecommunication Engineering, South China Normal University, Guangzhou 511411, People's Republic of China

(Received 1 December 2008; published 2 April 2009)

A relativistic many-body perturbation calculation is applied to calculate the hyperfine constants on the low-lying states of the alkaline-earth-metal ion $^{135}\text{Ba}^+$. Orbital energies and wave functions are calculated by solving Dirac equation. Zeroth-order hyperfine constants are calculated with Dirac wave functions. The finite basis sets of the Dirac equation are constructed by B splines. With the finite basis sets, the core polarization and the correlation effect are calculated for the hyperfine constants. The final results for $^{135}\text{Ba}^+$ are $a(6S_{1/2})=3754.813$ MHz, $a(6P_{1/2})=658.042$ MHz, $a(6P_{3/2})=109.383$ MHz, $b(6P_{3/2})=61.220$ MHz, $a(5D_{3/2})=180.649$ MHz, $b(5D_{3/2})=31.729$ MHz, $a(5D_{5/2})=-19.104$ MHz, and $b(5D_{5/2})=42.251$ MHz.

DOI: [10.1103/PhysRevA.79.042501](https://doi.org/10.1103/PhysRevA.79.042501)

PACS number(s): 32.10.Fn, 31.30.Gs

I. INTRODUCTION

With the development of experimental researches of the new optical frequency standards, studies of the hyperfine structure have become more and more important [1–3]. The hyperfine structure is caused by the interaction between the electrons and the electromagnetic multipole moments of the nucleus. Through the study of hyperfine structures, one can obtain both the information of nuclear structure and the electronic properties of atoms. During the last few decades, various experimental techniques, such as atomic-beam magnetic-resonance method [4–6], cascade anticrossing spectroscopy [7], and fast-ion-beam laser spectroscopy [8,9], have been used to measure the hyperfine structure of different atoms or ions. Simultaneously, many theoretical methods have been developed for accurate calculations on hyperfine interactions, including relativistic many-body perturbation theory (MBPT) [10], relativistic coupled-cluster method [11–13], multiconfiguration Dirac-Hartree-Fock, and relativistic configuration-interaction methods [14]. The effective operator form of many-body perturbation theory was developed and applied to calculate hyperfine structure by Garpman *et al.* [15,16]. An important task of a perturbation calculation is to carry out summations over all intermediate states. Lindgren and Morrison [16] used a single-particle function and a pair function by solving inhomogeneous one- and two-particle equations instead of the summations. However, in this paper, the finite basis sets of the Dirac equation are constructed by B splines. With the finite basis sets, the core polarization and the correlation diagrams are calculated, and the hyperfine constants on the low-lying states of $^{135}\text{Ba}^+$ are obtained. In our former work, we have obtained the hyperfine constants of $^{43}\text{Ca}^+$ and $^{87}\text{Sr}^+$ [17].

II. THEORY AND METHOD

For single-electron systems outside closed shells, the generalized hyperfine structure constants are [18]

$$A_K = \langle \gamma jj | T_0^{(K)} | \gamma jj \rangle M_0^{(K)} = \begin{pmatrix} j & K & j \\ -j & 0 & j \end{pmatrix} \langle \gamma j || T^{(K)} || \gamma j \rangle M_0^{(K)}. \quad (1)$$

For the magnetic-dipole hyperfine constant $K=1$, and for the electric quadrupole $K=2$. In the relativistic case, we get the traditionally used hyperfine constants,

$$a = \frac{A_1}{I_j} = \frac{\mu_I}{I_j} \langle \gamma jj | T_0^{(1)} | \gamma jj \rangle = \frac{\mu_I}{I_j} \begin{pmatrix} j & 1 & j \\ -j & 0 & j \end{pmatrix} \langle j || T^{(1)} || j \rangle, \quad (2)$$

$$b = 4A_2 = 2Q \langle \gamma jj | T_0^{(2)} | \gamma jj \rangle = 2Q \begin{pmatrix} j & 2 & j \\ -j & 0 & j \end{pmatrix} \langle j || T^{(2)} || j \rangle, \quad (3)$$

where I , μ_I , and Q are the nuclear spin, magnetic-dipole moment, electric-quadrupole moment, and j is the total angular momentum of the electrons, respectively.

In order to evaluate second- and third-order perturbation diagrams, a complete set of single-particle states is needed. We construct a complete finite basis set of the Dirac equation by B splines.

The relativistic Hamiltonian for an atomic system is given by

$$H = H_0 + V, \quad (4)$$

where

$$H_0 = \sum_{i=1}^N [c\alpha_i p_i + (\beta_i - 1)c^2 + V_{\text{nuc}}(r_i)] + \sum_{i=1}^N u(r_i), \quad (5)$$

and

$$V = \sum_{i < j} \frac{1}{r_{ij}} - \sum_{i=1}^N u(r_i). \quad (6)$$

Then the large and small component radial wave functions are expanded in terms of B splines of order k as

$$P_\kappa(r) = \sum_{i=1}^n p_i^{(\kappa)} B_{i,k}(r), \quad Q_\kappa(r) = \sum_{i=1}^n q_i^{(\kappa)} B_{i,k}(r). \quad (7)$$

Using the Galerkin method and the MIT-bag-model boundary condition, we obtain a $2n \times 2n$ symmetric generalized eigenvalue equation [19],

$$Av = \epsilon Bv, \quad (8)$$

where the $2n$ -vector v is given by

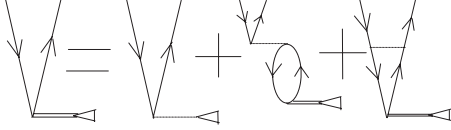


FIG. 1. The core polarization iterative diagram.

$$v = (p_1, p_2, \dots, p_n, q_1, q_2, \dots, q_n), \quad (9)$$

and A is a symmetric $2n \times 2n$ matrix with the form

$$A = \begin{pmatrix} (V_d) + (V_{\text{ex}}^{PP}) & c[(D) - (\kappa/r)] + (V_{\text{ex}}^{PQ}) \\ -c[(D) + (\kappa/r)] + (V_{\text{ex}}^{PQ}) & (V_d) - 2c^2(C) + (V_{\text{ex}}^{QQ}) \end{pmatrix} + A', \quad (10)$$

where atomic units (a.u.) have been used in the above expressions.

Numerical techniques employing B splines are recognized as extremely powerful tools for computational problems in physics. Details of B splines can be found in the book of deBoor [20]. Johnson *et al.* applied the technique of constructing finite basis sets from B splines to calculate the hyperfine constants of the alkali metals ^7Li , ^{23}Na , ^{39}K , ^{85}Rb , and ^{133}Cs [21]. The formalism underlying our computational procedure can be found in Refs. [17,19].

Following Lindgren and Morrison [16], the contribution of the hyperfine interaction can be divided into two parts: core-polarization part and correlation part. The core polarization can be shown in Fig. 1.

After multiplying both sides in Fig. 1 with $(\varepsilon_a - \varepsilon_r)$, we get the following equation:

$$(\varepsilon_a - \varepsilon_r) \overline{h}_a^{r(N)} = \langle r || T^K || a \rangle + \sum_{bsk} [G_1 X^k(rb, as) - G_2 X^k(br, as)] \overline{h}_a^{r(N-1)} \quad (11)$$

and

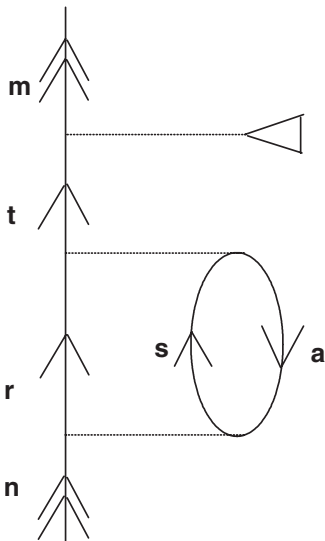


FIG. 2. One of the 65 lowest-order correlation diagrams.

TABLE I. Comparison of single-particle energies of $^{135}\text{Ba}^+$ with others. (B -spline parameter: $N=50$, $K_B=9$, $R_B=80$ a.u.; Nuclear Fermi charge distribution parameters: $t=2.3$ fm, $c=5.7476$ fm, root-mean-square nuclear radii $i=4.8377$ fm.)

States ^a	Others ^b (cm^{-1})	Ours (a.u.)	Ours (cm^{-1})
$6s$	75339	0.34327251	75339.597
$6p^-$	57265	0.26092106	57265.545
$6p^+$	55873	0.25457782	55873.365
$5d^-$	68138	0.31046422	68139.010
$5d^+$	67664	0.30830359	67664.807

^aNotation: $p^- = p_{1/2}$, $p^+ = p_{3/2}$, etc.

^bReference [23].

$$\overline{h}_a^{r(0)} = \frac{\langle r || T^K || a \rangle}{\varepsilon_a - \varepsilon_r}. \quad (12)$$

With Eqs. (11) and (12), we can use an iterative procedure to carry out the core polarization to all orders. The diagrams involving at least one double excitation are called correlations. The remaining third-order hyperfine diagrams are the lowest-order correlation diagrams. There are 65 such correlation diagrams.

One of these diagrams is shown in Fig. 2, and the algebraic expression is

$$\begin{aligned} \mathcal{D}(\text{Fig. 2}) &= \sum_{rsta} \frac{\langle m || T_Q^K || t \rangle \langle ta || r_{12}^{-1} || rs \rangle \langle rs || r_{12}^{-1} || na \rangle}{(\varepsilon_m - \varepsilon_t)(\varepsilon_n + \varepsilon_a - \varepsilon_r - \varepsilon_s)} \\ &= \sum_{rsta} \delta_{(j_t, j)} \frac{(2j_r + 1)(2j_a + 1)(2j_s + 1)}{2k + 1} \\ &\quad \times \begin{pmatrix} j & k & j_r \\ -1/2 & 0 & 1/2 \end{pmatrix}^2 \begin{pmatrix} j_a & k & j_s \\ -1/2 & 0 & 1/2 \end{pmatrix}^2 \\ &\quad \times \frac{\langle m || T^K || t \rangle R^k(ta, rs) R^k(rs, na)}{(\varepsilon_m - \varepsilon_t)(\varepsilon_n + \varepsilon_a - \varepsilon_r - \varepsilon_s)}. \end{aligned} \quad (13)$$

Where T_Q^K is the hyperfine operator, the other expressions, such as $R_Q^k(ta, rs)$, $X^k(rb, as, \dots)$ can be found in our former work [17]. From this expression, we can see that the sums run over all the virtual states of r , s , and t as well as core states of a . The property of two $3j$ symbols $\begin{pmatrix} j & k & j_r \\ -1/2 & 0 & 1/2 \end{pmatrix}$ and $\begin{pmatrix} j_a & k & j_s \\ -1/2 & 0 & 1/2 \end{pmatrix}$ gives $|j - j_r| \leq k \leq j + j_r$, $|j_a - j_s| \leq k \leq j_a + j_s$, $0 \leq j_r$, $j_s \leq \infty$, and $j_t = j$. In the above expression, $j_m = j_n = j$; the total angular momentum for the valence state is used. For numerical calculation it is impossible to take j_r, j_s up to infinity. We can choose a finite value j_{max} as the maximum and let $j_r, j_s \leq j_{\text{max}}$. But how can we choose j_{max} ? First we take a small positive floating number ε as the precision, and search using j_{try} to make the absolute value of the difference of the calculated results of the correlation diagram for two neighboring j_{try} less than ε . When we find such a j_{try} , we take this j_{try} as j_{max} . In our program, $\varepsilon=0.001$ and $j_{\text{max}}=10$ are used. We have used an iterative procedure to carry out the core polarization to all orders, and calculated all 65 lowest-order

TABLE II. Hyperfine factor a for different states of $^{135}\text{Ba}^+$ and $^{137}\text{Ba}^+$ (unit of MHz).

Isotope	State	$\frac{a}{\mu_I}$	a		
			Ours	Other	Expt.
$^{135}\text{Ba}^+$	$6s$	4479.294	3754.813	3718 ^a	3593.3(2.2) ^b
	$6p^-$	785.00942	658.042	621 ^a	664.6(0.3) ^c , 665.0(1.6) ^b
	$6p^+$	130.48815	109.383	112.4 ^a	113.0(0.1) ^c , 113.1(0.5) ^d
	$5d^-$	215.50474	180.649		169.5892(9) ^e
	$5d^+$	-22.79	-19.104		-10.735(2) ^e
$^{137}\text{Ba}^+$	$6s$	4343.425 ^f		4072.83 ^f	
	$6p^-$	785.944 ^f		736.98 ^f	
	$6p^+$	139.639 ^f		130.94 ^f	
	$5d^-$	201.301 ^f		188.76 ^f	
	$5d^+$	-19.196 ^e		-18 ^e	

^aReference [11].^bReference [24].^cReference [9].^dReference [25].^eReference [8].^fReference [12].

correlation diagrams one by one. In order to get higher precision, in our programs, we treated the atomic nuclei as Fermi nuclei [22], not point charges, and we used the Gauss integral which has higher precision in our program.

III. RESULTS AND DISCUSSION

In this paper we have calculated the Dirac-Fock single-particle energies of $^{135}\text{Ba}^+$ with the finite basis sets constructed by B splines. The results are given in Table I. In order to compare with others, we convert our results with the relation 1 a.u. = $2.194\,746 \times 10^5 \text{ cm}^{-1}$, and list the corresponding results in column 4. Comparing columns 2 with 4, we can see that our results of single-particle energies for

$^{135}\text{Ba}^+$ are in very close agreement with the recent data [23]. This indicates that the wave functions in this work are quite accurate and reliable to evaluate the core polarization and the correlation effects in the hyperfine interactions.

Table II shows the comparison of our evaluated hyperfine a constant results with other theoretical results and experimental results. In order to compare with the parameters of $^{137}\text{Ba}^+$, the factor of $\frac{a}{\mu_I}$ is also listed in Table II by $\mu_I(^{135}\text{Ba}) = 0.838\,26 \mu_N$ and $\mu_I(^{137}\text{Ba}) = 0.9377 \mu_N$, where μ_N is nuclear magnetron. From the table, we can see that our final results of $^{135}\text{Ba}^+$ are generally in good agreement with other calculations and with the available experimental data, with the exception of D states. Such status also occurs in $^{43}\text{Ca}^+$, $^{87}\text{Sr}^+$ [17], and $^{137}\text{Ba}^+$ [14]. The differences of the

TABLE III. Hyperfine factors b for different states $^{135}\text{Ba}^+$ and $^{137}\text{Ba}^+$.

Isotope	States	b/Q (MHz b ⁻¹)		b (MHz)	
		Ours	Others	Ours	Expt.
$^{135}\text{Ba}^+$	$6p^+$	382.625	373.5 ^a	61.220	59.4(2.3) ^b , 60.7(1.2) ^c
	$5d^-$	198.306		31.729	28.9536(25) ^d
	$5d^+$	264.069		42.251	38.688(10) ^d
$^{137}\text{Ba}^+$	$6p^+$		378 ^d		
	$5d^-$		193 ^d		
	$5d^+$		258 ^d		

^aReference [11].^bReference [24].^cReference [25].^dReference [8].

TABLE IV. Contributions from different parts of the hyperfine operator to the a factors of $^{135}\text{Ba}^+$ (unit of MHz). H(1) is the Dirac contribution, H(2) complete polarization, H(3) the lowest-order correlation, and the column headed "Final" is H(1)+H(2)+H(3).

States	H(1)	H(2)	H(3)	Final
$6s$	2638.931	479.466	636.416	3754.813
$6p^-$	441.681	85.853	130.508	658.042
$6p^+$	64.362	37.495	7.525	109.383
$5d^-$	114.824	13.613	52.212	180.649
$5d^+$	46.066	-85.676	20.505	-19.104

factor of $\frac{a}{\mu_I}$ between the present work on $^{135}\text{Ba}^+$ and others on $^{135}\text{Ba}^+$ are small. It is reasonable.

In Table III, we give out our calculated hyperfine structure b/Q values for $^{135}\text{Ba}^+$ in column 3. The results of the b values, of course, depend on the size of the nuclear quadrupole moment Q . However, there exists no experimental technique for determining nuclear quadrupole moments in a direct way. In order to compare our results to Experiments, $Q(^{135}\text{Ba}^+)=0.160 b$ [23] is used, where $1 b=1 \times 10^{-28} \text{ m}^2$, and the corresponding b constants are derived and listed in column 5, from which we can see that our result is compatible to the recent experiment results. Also we list the b/Q values for $^{137}\text{Ba}^+$ in column 4. Comparing to $^{135}\text{Ba}^+$, we can see that the difference between them are very small, just like the $\frac{a}{\mu_I}$. This is because of their similar atomic structure.

In order to discuss the different parts of the hyperfine constants, we listed the contributions from different parts of the hyperfine operator to the final results for the hyperfine structure constants a and b factors in Tables IV and V, respectively. H(1) is the Dirac-Fock contribution and H(2) is the complete polarization. In our work, H(2) is calculated to all order. From Table IV, we can see that, for $6S_{1/2}$, $6P_{1/2}$, and $5D_{3/2}$ states, H(2) are less than the lowest-order correlation H(3) but for $6P_{3/2}$ state H(2) is about five times of H(3). In particular, for the $5D_{5/2}$ state, the final result is relatively small and has the opposite sign, which seems to be caused by the complete polarization. Our final result of $D_{5/2}$ did not agree with the experiment. In fact, the theoretical results of $D_{5/2}$ states of different alkaline-earth-metal ions, such as

TABLE V. Contributions from different parts of the hyperfine operator to b factor of $^{135}\text{Ba}^+$ (unit of MHz). Notation is the same in Table IV.

States	H(1)	H(2)	H(3)	Final
$6p^+$	35.839	18.105	7.276	61.220
$5d^-$	21.369	3.775	6.584	31.729
$5d^+$	27.371	6.860	8.019	42.251

$^{43}\text{Ca}^+$, $^{87}\text{Sr}^+$ [17], and $^{137}\text{Ba}^+$ [14] did not agree with each other. H(3) is the lowest-order correlation. The column headed "Final" represents H(1)+H(2)+H(3).

From Table V, we can see that for $P_{3/2}$ state the complete polarization effect is larger than the correlation effect. But for $D_{3/2}$ and $D_{5/2}$ states, the complete polarization effects are less than the correlation effect.

In conclusion, in this work we have performed a relativistic MBPT calculation for $^{135}\text{Ba}^+$, where the single-particle energies and hyperfine constants are evaluated. The relativistic wave functions used in this work are quite accurate to calculate the core polarization and the correlation effect in the hyperfine interactions. In this work, we have calculated the core-polarization part to all orders and all the 65 lowest-order correlation diagrams. But in addition to these diagrams, there are numerous second- and higher-order correlation diagrams, which are rather time consuming to evaluate. It is impossible to use an iterative program to calculate all the second- or higher-order correlation diagrams so the principal discrepancy between our results and experiments is due to the uncalculated second- and higher-order correlation effects. It is believed that the accuracy of these calculations could be improved by including the second- and higher-order effects, which we are now trying to do. We hope that our theoretical results will be useful for analyzing future experiments.

ACKNOWLEDGMENTS

The author would like to thank Wu Li-jin and Shi Ting-yun for their useful help. This work is supported by the National Natural Science Foundation of China under Grant No. 10747131.

[1] A.-M. Martensson-Pendrill, J. Phys. B **35**, 917 (2002).
 [2] G. P. Barwood, K. Gao, P. Gill, G. Huang, and H. A. Klein, Phys. Rev. A **67**, 013402 (2003).
 [3] V. Gerginov, K. Calkins, C. E. Tanner, J. J. McFerran, S. Diddams, A. Bartels, and L. Hollberg, Phys. Rev. A **73**, 032504 (2006).
 [4] M. L. Perl, I. I. Rabi, and B. Senitzky, Phys. Rev. **98**, 611 (1955).
 [5] P. Buck and I. I. Rabi, Phys. Rev. **107**, 1291 (1957).
 [6] S. M. Heider and G. O. Brink, Phys. Rev. A **16**, 1371 (1977).
 [7] K. H. Liao, L. K. Lam, R. Gupta, and W. Happer, Phys. Rev.

Lett. **32**, 1340 (1974).
 [8] R. E. Silverans, G. Borghs, P. De Bisschop, and M. Van Hove, Phys. Rev. A **33**, 2117 (1986).
 [9] P. Villemoes, A. Arnesen, F. Heijkenskjold, and A. Wannstrom, J. Phys. B **26**, 4289 (1993).
 [10] S. Ahmad, J. Andriessen, K. Raghunathan, and T. P. Das, Phys. Rev. A **25**, 2923 (1982).
 [11] A.-M. Martensson-Pendrill and A. Ynnerman, J. Phys. B **25**, L551 (1992).
 [12] B. K. Sahoo, G. Gopakumar, R. K. Chaudhuri, B. P. Das, H. Merlitz, U. S. Mahapatra, and D. Mukherjee, Phys. Rev. A **68**,

- 040501(R) (2003).
- [13] B. K. Sahoo, R. Chaudhuri, B. P. Das, and D. Mukherjee, Phys. Rev. Lett. **96**, 163003 (2006).
- [14] W. M. Itano, Phys. Rev. A **73**, 022510 (2006).
- [15] S. Garpman, I. Lindgren, T. Lindgren, and J. Morrison, Phys. Rev. A **11**, 758 (1975).
- [16] I. Lindgren and J. Morrison, *Atomic Many-Body Theory*, Springer Series in Chemical Physics (Springer, Berlin, 1982).
- [17] K. Z. Yu, L. J. Wu, B. C. Gou, and T. Y. Shi, Phys. Rev. A **70**, 012506 (2004).
- [18] I. Lindgren and A. Rosen, Case Stud. At. Phys. **4**, 93 (1974).
- [19] W. R. Johnson, S. A. Blundell, and J. Sapirstein, Phys. Rev. A **37**, 307 (1988).
- [20] C. deBoor, *A Practical Guide to Splines* (Springer, New York, 1978).
- [21] W. R. Johnson, M. Idrees, and J. Sapirstein, Phys. Rev. A **35**, 3218 (1987).
- [22] F. A. Parpia and A. K. Mohanty, Phys. Rev. A **46**, 3735 (1992).
- [23] K. Beloy, A. Derevianko, V. A. Dzuba, G. T. Howell, B. B. Blinov, and E. N. Fortson, Phys. Rev. A **77**, 052503 (2008).
- [24] K. Wendt, S. A. Ahmad, F. Buchinger, A. C. Mueller, R. Neugart, and E. W. Otten, Z. Phys. A **318**, 125 (1984).
- [25] H. Winter and M. H. Gaillard, J. Phys. B **10**, 2739 (1977).